Bloch mode excitation in two-dimensional photonic crystals imaged by Fourier optics

A. Berrier,[1] M. Swillo,[1] N. Le Thomas,[2] R. Houdré,[2] and S. Anand[1,*]
[1]*Department of Microelectronics and Applied Physics, Royal Institute of Technology (KTH), Electrum 229, S-16440 Kista, Sweden*
[2]*Institut de Photonique et d'Electronique Quantique, École Polytechnique Fédérale, CH-1015 Lausanne, Switzerland*
(Received 2 July 2008; revised manuscript received 13 March 2009; published 23 April 2009)

Coupling into the Bloch modes of a two-dimensional photonic crystal (PhC) field is investigated by Fourier optics. The PhC was designed to operate in the second band above the air-light line, close to the autocollimation regime for TE polarization. The sample was fabricated in an InP-based heterostructure and an access ridge waveguide provides in-plane excitation of the PhC. The spatial Fourier transform of the field maps obtained from finite-difference time-domain simulations and those calculated by plane-wave expansion are compared to the experimentally obtained equifrequency surfaces (EFS). The shape of the imaged EFS and its variation with the excitation wavelength is shown to be consistent with the theoretical simulations. Finally, the results indicate that if combined with different excitation geometries, Fourier optics can be a powerful technique to assess photonic crystal devices and to design efficient structures.

DOI: 10.1103/PhysRevB.79.165116 PACS number(s): 42.70.Qs, 42.30.Kq, 42.25.Bs

I. INTRODUCTION

Photonic crystals (PhCs) are electromagnetic structures with many interesting optical properties. New device concepts have been proposed and novel physical phenomena have been demonstrated experimentally. At first mainly used for their reflecting and light confining properties in devices such as waveguides or cavities, photonic crystals are now receiving significant attention for their unconventional light dispersion properties in the bands above the band gap. When light is coupled into the second band, phenomena such as superprism effect,[1,2] ultrarefraction,[3] autocollimation,[4] and negative refraction[5,6] were predicted and experimentally demonstrated. The different phenomena are determined by the shape and curvature of the band into which light is coupled, i.e., the shape of the equifrequency surfaces (EFSs) (Ref. 4) at the corresponding wavelength of light. It is therefore necessary to be able to measure the shape of the EFS to ensure the functionality of the fabricated PhC structures. Moreover, several bands associated with different k vectors may be available in the operating wavelength range and should be taken into account in the design for efficient operation. It is therefore central to investigate the coupling into Bloch modes and the role of the different available bands. However, there are hitherto only a few reports on the multiband coupling.[7]

In the case of two-dimensional (2D) photonic crystals (2D PhCs), light propagating in the plane of periodicity (in-plane modes) for which the wave vector $\boldsymbol{k}$ (modulo, a reciprocal-lattice vector $\boldsymbol{G}$) is shorter than the wave vector in air $\boldsymbol{k_0}$ can couple to radiative modes in air resulting in out-of-plane radiation of light. The wave vectors of the in-plane and out-of-plane modes are related.[8] Thus the light-radiated out of plane can convey information about the propagation of modes inside the PhC slab.[8] We address here the excitation of Bloch modes in a two-dimensional photonic crystal with a triangular lattice of air holes, operating in the second band at telecommunication wavelengths (around 1.5 μm). The sample was fabricated in an InP-based heterostructure and a 1.2-μm-wide access ridge waveguide provides the in-plane excitation of the PhC. The observation of the out-of-plane diffracted light in the Fourier plane of a lens is a fast and versatile method to obtain information about the in-plane propagating light.[8,9] Here it is used to characterize light propagation in photonic crystal fields designed for the operation in the second band above the light line. The spatial Fourier transform (FT) of the field maps obtained from finite-difference time-domain (FDTD) simulations and those calculated by the plane-wave expansion (PWE) are compared to the EFS obtained by Fourier optics. This allows unambiguously to identify the excited Bloch modes. We then discuss the obtained experimental data taking into account the simulation results.

II. THEORETICAL

We consider PhC fields composed of a 2D triangular lattice of air holes in an InP/InGaAsP/InP heterostructure slab waveguide. Mode guiding in the direction perpendicular to the slab (i.e., parallel to the PhC holes) is accounted for by using the effective index method giving an effective refractive index $n_{\mathrm{eff}}=3.24$ for the fundamental mode. We consider TE polarization (i.e., with the E-field perpendicular to the PhC holes) and design the PhC to operate above the band gap. PWE (Ref. 10) is used to calculate the band structure for wave vectors in the full first Brillouin zone (FBZ). Figure 1 displays the EFSs in the reciprocal space for TE polarization at the normalized frequency $u=a/\lambda=0.310$,where a is the period of the PhC lattice and λ the wavelength of light. Reciprocal-lattice points of the PhC structure are indicated by black dots. The closed shapes around the reciprocal-lattice points are the EFS corresponding to the second band. The trigonal shapes correspond to the third band. The equifrequency contours indicate the position in reciprocal space of the available Bloch modes actually supported by the considered PhC at the given wavelength. However, the Bloch modes propagating in the PhC field are the group of available modes excited by the input light. The angular distribution of input wave vectors is determined by the geometry of the input light coupling (e.g., numerical aperture of the

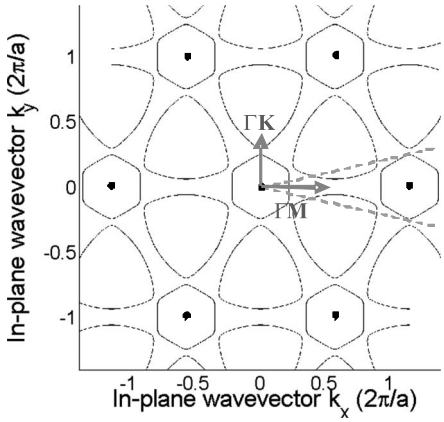

FIG. 1. Equifrequency contours for $u=0.310$ as calculated from the plane-wave expansion with $r/a=0.195$ and the dielectric constant of the background material $\varepsilon_b=10.5$. The second and third bands are represented for TE polarization. The black dots are the reciprocal-lattice points. The area between the dashed gray lines indicates one possible momentum distribution of the input light required to excite the complete distribution of available Bloch modes for an operation in the second band. ΓM and ΓK directions are also indicated.

ridge). The dotted straight lines on Fig. 1 illustrate schematically an example of wave-vector distribution $\boldsymbol{k}_{\text{in}}$ for the input light in the ΓM direction. Among all the available Bloch modes along the EFS, the excited Bloch modes in the first Brillouin zone are represented by a function $B^{(n)}(\boldsymbol{k})$ with n as the band number and $\mathbf{k}$ as the wave vector. This function corresponds, in the first Brillouin zone, to the part of the EFS which is excited. The extent of this function along the EFS depends on the coupling geometry. The complete solution for the nth band in the full reciprocal space is the function $B^{(n)}_{\text{full}}(\boldsymbol{k})$, which can be seen as a periodic repetition of $B^{(n)}(\boldsymbol{k})$ according to the reciprocal lattice. The Fourier transform of the electromagnetic field in the PhC corresponding to band n is given by $B^{(n)}_{\text{full}}(\boldsymbol{k})$ multiplied by a weight function $V^{(n)}_G(\boldsymbol{k})$. The $V^{(n)}_G(\boldsymbol{k})$ are the Fourier coefficients occurring in the plane-wave expansion of the Bloch wave $\varphi^{(n)}(\boldsymbol{r},\boldsymbol{k})$. That is,

$$\varphi^{(n)}(\boldsymbol{r},\boldsymbol{k}) = \left\{ \sum_G V^{(n)}_G(\boldsymbol{k}) \exp[j(\boldsymbol{G}+\boldsymbol{k}) \cdot \boldsymbol{r}] \right\}, \tag{1}$$

where $\mathbf{G}$ is a reciprocal-lattice vector, and $\boldsymbol{r}$ is a real-space vector. The Fourier coefficient function $V^{(n)}_G(\boldsymbol{k})$ describes the repartition of the energy of each Bloch mode into its different components located in the different Brillouin zones (power spectrum). It has been shown earlier that in the case of operation in bands above the band gap, the dominant Fourier harmonics are located outside the first Brillouin zone.[11] Therefore, the signal has its maximum around one reciprocal-lattice point away from the origin. The values of the different Fourier coefficients in Eq. (1) can be calculated by PWE and depend on the dielectric constant function $\varepsilon(\boldsymbol{r})$ of the photonic crystal (e.g., refractive index contrast and air-fill factor).

The excitation of the Bloch modes [functions $B^{(n)}(\boldsymbol{k})$] is a measure for the light coupling into the PhC structure and depends on the geometry of excitation (size, position of the ridge, etc.). In order to access this information, we simulated the field map in the PhC field by 2D FDTD using the freeware F2P (Ref. 12) and then calculated the spatial Fourier transform of the field map [Fourier transform finite-difference time domain (FT-FDTD)].[13] Phase information about the FDTD calculated field map is retrieved by considering values at times t and t-λ/4c where λ is the wavelength and c is the velocity of light. The geometrical structure used for the calculations is a PhC field ($r/a=0.195$, with r as the radius of the PhC holes and a as the lattice parameter) of length 30 μm with a ridge waveguide located close to the PhC interface as shown on Fig. 2(a). The corresponding FT-FDTD map is displayed on Fig. 2(b) in the full reciprocal space (in the range $[-1.2;1.2]2\pi/a$). The Bloch harmonics carrying most of the energy belong to Brillouin zones situated around the first Brillouin zone, hence a small incident angle of k values in the FBZ is sufficient to excite most of the available Bloch modes as shown on Fig. 1. Figure 2(b) represents the expansion of the Bloch modes propagating in the PhC field. The signal is strong in the Brillouin zones where the Fourier coefficients are significant. In the other Brillouin zones, the signal is weaker. Figure 2(c) presents a plot of the FT-FDTD signal as a function of k_x at $k_y=0$. The signal intensity in the FBZ [for k_x around $-0.24(2\pi/a)$] is only about 4% of the maximum signal intensity.

The distance from the ridge to the PhC does not influence the distribution of incoming k vectors; however, it influences the number of holes illuminated at the PhC interface. When the ridge is very close to the PhC, the few illuminated holes will interact strongly with the incident field and redistribute the incoming light. One notes here that a point-source excitation located inside the PhC field would allow the experimental recovery of a wider part of the EFSs owing to the larger angular distribution of input wave vectors.

If one considers the EFS for the second band in the FBZ, the intersection with the light cone is found for $u=0.28$. Therefore for larger values of u, the component of the excited Bloch modes in the FBZ is located inside the light cone and thus gives rise to the out-of-plane scattering to air. The collection of the light radiating out of the PhC field allows the experimental measurement of the product $B^{(n)}_{\text{col}}(\boldsymbol{k})V^{(n)}_0(\boldsymbol{k})$ where $B^{(n)}_{\text{col}}(\boldsymbol{k})$ is the part of the excited EFS situated above the light line and collected by the objective. We note here that in the range $u=0.30$ to 0.36 (second band above the air-light line), the most energetic component of the Bloch modes allowed in the PhC field is located in the Brillouin zones immediately surrounding the FBZ. Since out-of-plane radiation is limited to the component inside the light cone in the FBZ, it will carry relatively little energy as seen on Fig. 2(b). As a consequence, even though we are working at frequencies above the light line, most of the light is propagating in the PhC field without suffering appreciable out-of-plane losses.

Figure 3 shows the harmonics of the excited Bloch modes located in the FBZ, where it is compared to the EFS calculated by PWE. The FT-FDTD calculations (Fig. 3) indicate that Bloch modes from more than one band (in our particular case, second and third bands) can be excited in the PhC field; this leads to the presence of coexisting Bloch waves travel-

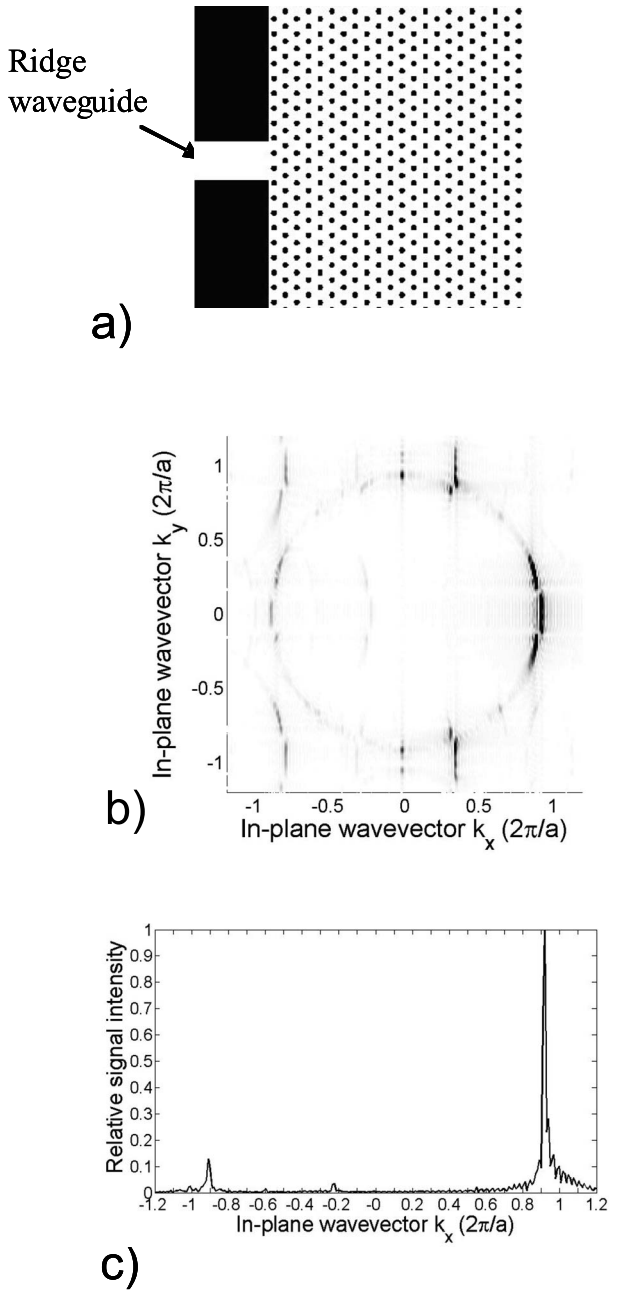

FIG. 2. (a) Schematic sketch of the simulated configuration showing the access ridge waveguide and the PhC field; (b) Fourier transform of the field maps calculated by FDTD in the PhC field for $u=0.31$ (TE polarization). The geometry is as shown in (a). The contrast has been increased for better visibility. (c) Variation in the FT-FDTD signal as calculated as a function of k_x (at $k_y=0$).

ing with several different group velocities. This is a phenomenon referred to as multirefringence effect.[14,15] However, for a device designed to operate in, e.g., the second band, coupling to more than one band will induce a loss of energy into modes that are not practically useful or that are undesirable. The presence of the third band in the operating range depends on the nature of the PhC (geometrical parameters such as lattice constant, etc., and dielectric constant) and, if needed, one can design structures in such a way that the third band is absent from the EFSs in a large frequency range.

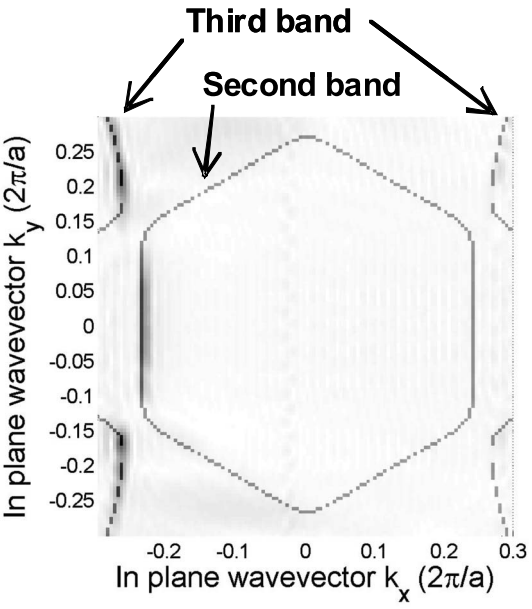

FIG. 3. FT-FDTD calculations for the geometry of Fig. 2(a) and for $u=0.310$ (TE polarization). Also shown for comparison are the EFS obtained by PWE (lines).

III. EXPERIMENTAL

The epitaxial structure was grown by metal organic vapor phase epitaxy with a 200 nm InP cladding layer and a 434 nm InGaAsP core layer on InP. The PhCs patterns were generated by electron-beam lithography using ZEP520 as the resist then transferred into the SiO_2 mask by fluorine-based reactive ion etching. Then the samples were etched by Ar/Cl_2 chemically assisted ion-beam etching.[16] The lattice period is $a=465$ nm and the hole diameter 190 nm as measured from scanning electron microscopy (SEM). ΓM oriented 30-μm-long PhC fields are coupled to a deeply etched ridge waveguide (Fig. 4) placed close to the PhC field.

The optical characterization was performed in an end-fire configuration using microlensed fibers to couple light into the access ridge waveguides. A polarizer at the input is used to ensure TE polarization. The out-of-plane light is collected by a microscope objective with a numerical aperture NA $=0.95$ and a focal length $f=1.3$ mm. A detailed description of the experimental setup can be found in Ref. 8. A tunable laser operated in the range 1480–1620 nm is used as the source. The optics is configured to form an image on an

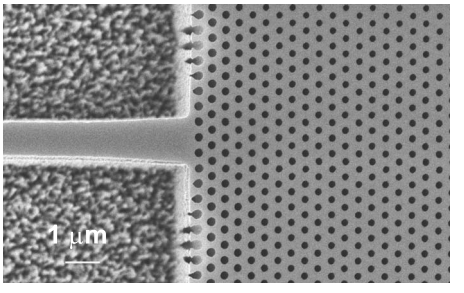

FIG. 4. Scanning electron microscope top view of the fabricated PhC structure close to the input interface.

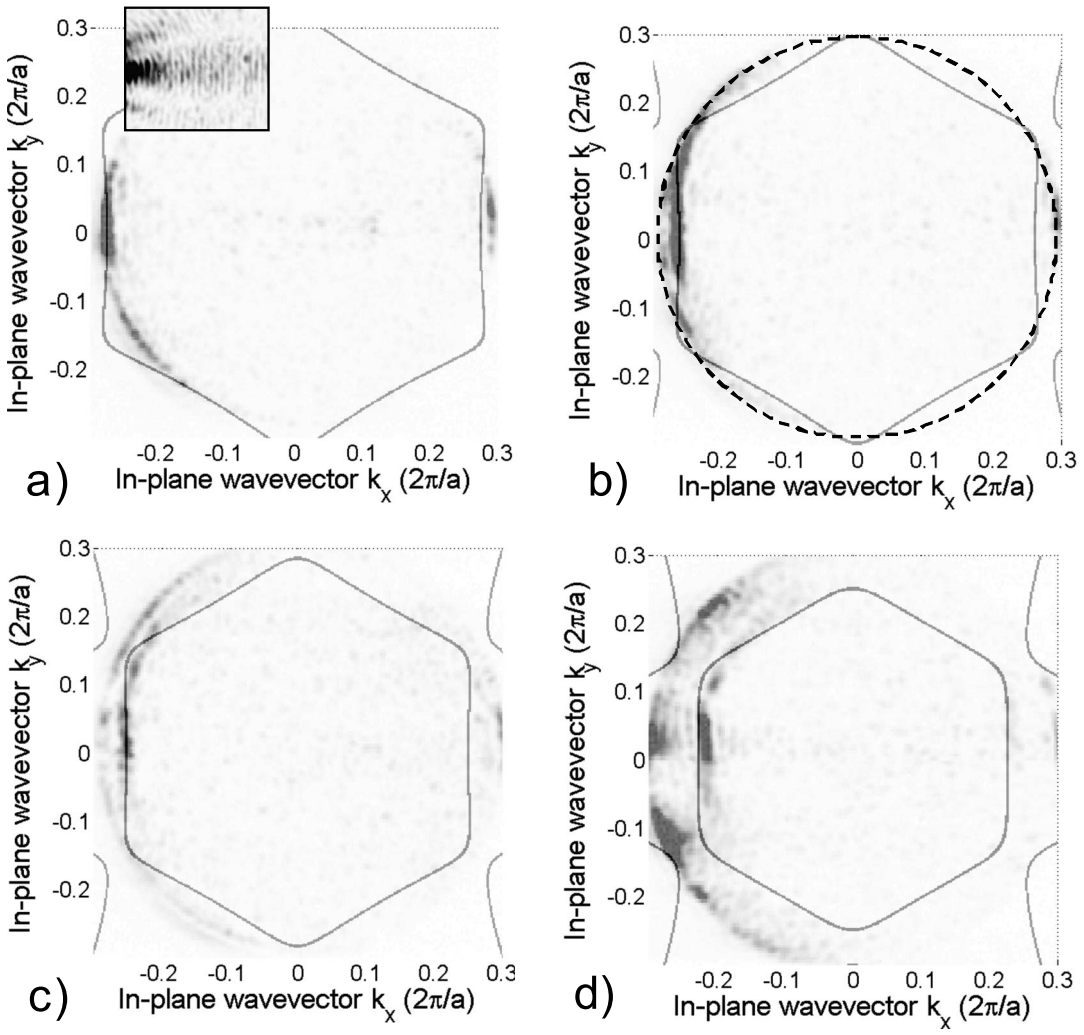

FIG. 5. In-plane wave vectors determined experimentally from the Fourier images compared with the EFS calculated by PWE (fine line) (a) $u=0.300$, (b) $u=0.305$, (c) $u=0.310$, and (d) $u=0.315$. In the inset of (a) is the real-space image of the light propagating in the PhC field indicating autocollimation. In (b), the circular dotted line indicates the border of the pupil.

InGaAs charge-coupled device (CCD) camera either of the sample surface (real-space configuration) or of the back focal plane of the objective providing the optical Fourier transform of the collected out-of-plane radiation (reciprocal space configuration).[9] We consider the collecting objective as a thick lens and within the Abbe sine condition, we can express the distances in the Fourier plane as

$$d = |k_{\text{in}}| \frac{a}{2\pi} \frac{f}{u}. \tag{2}$$

The Fourier plane is subsequently imaged on the CCD camera. The image on the CCD camera is thus a direct observation of the in-plane wave vectors of the plane-wave components of the excited Bloch modes in the PhC field. We record Fourier plane images within the normalized frequency range $u=0.30$ to 0.315. We calibrate the distances on the CCD recorded image and use the obtained conversion factor together with the scaling law of Eq. (2) to obtain the in-plane wave vectors k_{in}. The calibration between the CCD pixels and the scale of reciprocal space is obtained from measurements on gratings.[17] These results are then compared to the EFSs calculated by PWE.

IV. RESULTS AND DISCUSSION

The experiments were performed for different wavelengths in the range 1480–1620 nm. Figure 5 shows some representative measurements together with the EFSs obtained from PWE for $u=0.300$, 0.305, 0.310, and 0.315, for TE polarization. The numerical aperture of the microscope objective is indicated by a dotted circle superposed on the data on Fig. 5(b) and represents the limit angle for light collection (border of the pupil). The light present in the region indicated by the dotted circle is due to the light scattered from the interfaces. In the investigated range, the shape of the EFS in the ΓM direction is flat and indicates a regime of autocollimation. This is also supported by the observed real-space image of the light propagating in the PhC (inset of Fig. 5(a)]. The apparent dispersion at the left edge of the image is due to the scattering at the input PhC or air interface.

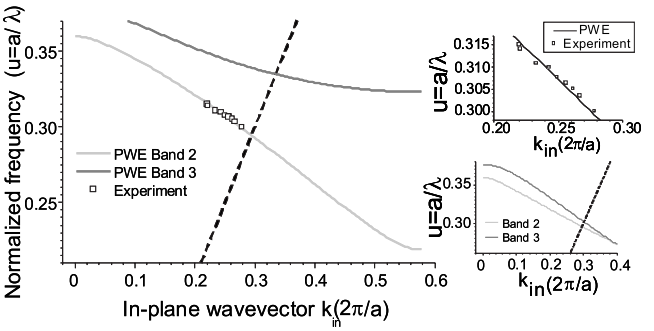

FIG. 6. (a) Second and third photonic TE bands as calculated by PWE in the ΓM direction. The open squares are the experimental points. (b) Close view of the the second band in the experimental wavelength range. (c) Second and third photonic bands (TE) in the ΓK direction. The light line (dashed line) is also shown on (a) and (c).

The calculated (PWE) Bloch modes belonging to the third band are visible in the corners of Figs. 5(b)–5(d). However, these modes are outside the range delimited by the numerical aperture of the objective. On the bottom left corner of Fig. 5(d), the higher intensity at the position of the third band (at the very edge of the objective line) suggests that the detected light might come from modes from the third band. It cannot be unambiguously attributed to the third band since it appears at the border of the pupil. As the wavelength is decreased, the EFS feature from the second band is clearly moving toward the center of the field of observation, which agrees very well with the positions of the EFS calculated by PWE. The wavelength dependence of the position in k space of the experimental signal along the x axis is compared to the PWE calculated band structure in the ΓM direction [Fig. 6(a)] The position of the light line is also indicated. At a given wavelength, the norm of the wave vector in the ΓM direction is obtained from the pixel difference between the origin of the reciprocal space and the measured signal. Thus for each measurement, we obtain the norm of k_x for the corresponding normalized frequency. Figure 6(b) shows a detailed view of the experimental data. The agreement in the position of the EFS as well as the slope of the second band is very good in the whole investigated range. Figure 6(c) displays the second and third bands, which are both oriented upward around the Γ point. This figure also illustrates that for the investigated range of normalized frequencies, the second band is associated with shorter wave vectors and is therefore first seen within the collection area.

Beside the determination of the slope of the second band, the present measurements are appropriate to determine the repartition of the propagating Bloch modes. The comparison of the experiments (Fig. 5) with the FT-FDTD calculations (Fig. 3) indicates that the experimental extent of the Bloch mode function $B^{(2)}(\boldsymbol{k})$ agrees qualitatively well with what is expected from FT-FDTD. If one excludes the scattering signal at the border of the pupil, the maximum of the collected signal corresponds to modes predicted by PWE. FT-FDTD calculations (Fig. 3) show that the excited Bloch modes belong to left side of the EFS contour associated with the second band. Only the Bloch waves located on the side of the EFS hexagon normal to the ΓM direction can carry energy, whereas those located on the other sides of the hexagon are not excited. The present configuration using an input ridge waveguide to couple the light into the PhC field couples to Bloch modes from the second band only on one side of the EFS hexagon, as is observed experimentally. In the present case, we excite all the accessible Bloch modes of the second band.

The results presented here indicate that FT-FDTD and PWE calculations together with Fourier optics can be used to design efficient coupling into PhC structures. The study of different excitation geometries with Fourier optics brings information about the scattered light as well as the Bloch modes into which light is preferentially coupled, thus allowing comparison of different interface designs. In addition, the method allows the determination of the excited photonic band as well as the effective refractive index and the distribution of the propagating wave vectors, including evanescent waves. Even though the experimental technique presented here is mostly appropriate to PhC structures operating in the transmission bands, it can also be advantageously applied to the investigation of coupling into diverse photonic waveguides.[17]

V. CONCLUSION

In conclusion, we presented an experimental investigation of the distribution of excited Bloch modes in a PhC field. The EFSs obtained by Fourier optics provide information on the behavior of the Bloch modes as the input wavelength is varied. The experimental data is in good agreement with calculated momentum space distributions retrieved by Fourier transforms of field maps calculated by FDTD and allows the assessment of the range of experimentally accessible k vectors for a given structure design. PWE calculated EFSs were used to show that the observed (excited) Bloch modes belong to the second band. The characterization technique based on Fourier optics cannot only be used as a powerful technique to assess photonic crystal devices but also for designing efficient coupling into PhC structures

ACKNOWLEDGMENTS

This work was supported by the Swedish Research Council (VR) and the European Network of Excellence on Photonic Integrated Components and Circuits (ePIXnet) and the Swiss NCCR-Quantum Photonics.

*anand@kth.se

[1] H. Kosaka, T. Kawashima, A. Tomita, M. Notomi, T. Tamamura, T. Sato, and S. Kawakami, Phys. Rev. B **58**, R10096 (1998).
[2] L. Wu, M. Mazilu, T. Karle, and T. F. Krauss, IEEE J. Quantum Electron. **38**, 915 (2002).
[3] D. Bernier, E. Cassan, A. Lupu, G. Maire, D. Marris-Morini, L. Vivien, and S. Laval, Opt. Commun. **274**, 241 (2007).
[4] V. Zabelin, L. A. Dunbar, N. Le Thomas, R. Houdré, M. V. Kotlyar, L. O'Faolain, and T. F. Krauss, Opt. Express **32**, 530 (2007).
[5] M. Notomi, Phys. Rev. B **62**, 10696 (2000).
[6] A. Berrier, M. Mulot, M. Swillo, M. Qiu, L. Thylen, A. Talneau, and S. Anand, Phys. Rev. Lett. **93**, 073902 (2004).
[7] J. Witzens, M. Hochberg, T. Baehr-Jones, and A. Scherer, Phys. Rev. E **69**, 046609 (2004).
[8] N. Le Thomas, R. Houdré, M. V. Kotlyar, D. O'Brien, and T. F. Krauss, J. Opt. Soc. Am. B **24**, 2964 (2007).
[9] G. Bartal, O. Cohen, H. Buljan, J. W. Fleischer, O. Manela, and M. Segev, Phys. Rev. Lett. **94**, 163902 (2005).
[10] K. M. Ho, C. T. Chan, and C. M. Soukoulis, Phys. Rev. Lett. **65**, 3152 (1990).
[11] B. Lombardet, L. A. Dunbar, R. Ferrini, and R. Houdré, J. Opt. Soc. Am. B **22**, 1179 (2005).
[12] www.imit.kth.se/info/FOFU/PC/F2P
[13] I. De Leon and F. S. Roux, Phys. Rev. B **71**, 235105 (2005).
[14] R. Zengerle, J. Mod. Opt. **34**, 1589 (1987).
[15] P. St. J. Russell, Appl. Phys. B **39**, 231 (1986).
[16] A. Berrier, M. Mulot, A. Talneau, R. Ferrini, R. Houdré, and S. Anand, J. Vac. Sci. Technol. B **25**, 1 (2007).
[17] N. Le Thomas, R. Houdré, L. H. Frandsen, J. Fage-Pedersen, A. V. Lavrinenko, and P. I. Borel, Phys. Rev. B **76**, 035103 (2007).